Comparative Study of Physicochemical Properties and Antibiofilm Activity of Graphene Oxide Nanoribbons

Javanbakht T.*[0000-0002-2658-330X], Hadian H., Wilkinson K. J.

University of Montreal, 2900 Edouard-Montpetit Blvd, H3T 1J4, Montreal, Quebec, Canada

Abstract. In this article, the antibiofilm activity and physicochemical properties of graphene oxide (GO) nanoribbons, which have been among the most exciting materials, were studied by measuring the ratio of killed to alive bacteria incubated with these nanomaterials. Our objective was to determine the related physicochemical and antibiofilm properties of graphene oxide nanoribbons. We hypothesized that the physicochemical properties of graphene oxide nanoribbons could affect their antibiofilm activity. A combination of spectroscopic and microscopic measurements of the samples allowed us to determine their physicochemical properties affecting the biofilms. Our work includes information on the surface properties of these materials related to their incubation with the biofilms. The Fourier transform infrared spectroscopy showed the vibrations of OH groups of water molecules adsorbed on graphene oxide nanoribbons. The results show the high antibiofilm activity of the graphene oxide nanoribbons. The fluorescence confocal microscopy revealed that 50 % ± 3 % of the total number of bacteria were killed with these nanomaterials. The incubation of graphene oxide nanoribbons with bacterial biofilms resulted in the appearance of the NO_2^-, NO_3^- peaks in the negative mode mass spectrum. The attenuation of the O^- and OH^- peaks were attributed to the interactions of the samples with the biofilms. Our study gives more evidence of the practical value of graphene oxide nanoribbons in killing bacteria related to their surface physical properties and the potential of these nanomaterials for materials science and biomedical applications.

Keywords: nanomaterials, bacterial biofilm, Fourier transform, infrared spectroscopy, transmission electron microscopy, time-of-flight secondary ion mass spectrometry, confocal microscopy.

1 Introduction

The materials science has attracted many researchers in recent years. Nanomaterials are among the materials that have unusual physical and biological properties. These specific materials have a size of less than 100 nm, which gives the unique advantage of penetration to small biosystems such as bacterial biofilms.

The emergence of multi-drug-resistant bacteria is a great challenge for which several antibiotics have been used both inside and outside of medicine. Microorganism, such as bacteria, can survive exposure to an antibiotic due to their antibiotic resistance [1, 2].

The ability of bacteria to develop antibiotic resistance and colonize biotic surfaces by forming biofilms is a great challenge for public health and the environment. Most infections causing bacteria in hospitals are resistant to at least one of the drugs most used for treatment. Some

microorganisms are resistant to all approved antibiotics, and they can only be treated with toxic drugs [3].

Nanomaterials have shown excellent potential for killing bacteria in recent research works. The bactericidal effects of these materials depend on their size and structure.

Graphene nanoribbons are carbon-based nanomaterials that have attracted attention in the recent decade due to their appropriate properties such as flexibility and outstanding heat conductivity. Graphene oxide (GO) nanoribbons are the oxidized products of graphene nanoribbons with a similar composition. Although these nanomaterials have been studied during recent years, their surface properties have not been wholly related to their antibiofilm properties. The change in the surface properties of these nanomaterials due to their incubation with bacterial biofilms is a critical issue to be investigated.

2 Literature Review

Bacterial biofilm is a three-dimensional microenvironment that efficiently protects the bacteria with a diverse physical structure composed of the extracellular polymeric substances (EPS) in the matrix, such as polysaccharides, proteins, nucleic acids, and lipids [4, 5]. For example, Streptococcus has neutral polysaccharides [6], whereas Pseudomonas and Staphylococcus have polyanionic and polycationic polysaccharides, respectively [7, 8]. The EPS are even diverse within a species of bacteria. For example, polysaccharides from various strains of Streptococcus thermophilus have different monomer compositions and ratios and possess different molecular masses [9]. The different interactions, synergistic or antagonistic, between members of the bacterial communities in the biofilm, can shift the bacterial population from health to disease [10].

Graphene nanoribbons are the strips of graphene with a high length-to-width ratio and straight edges [11]. Microfabrication on graphite surfaces followed by exfoliation has been used for the preparation of graphene [12]. Other techniques for the preparation of graphene are as follows: exfoliation of bulk graphite in the presence of surfactants [13], or plasma etching of multiwalled carbon nanotubes (MWCNTs) in a layer of the protective polymer [14].

Because of the oxygen-containing functionalities such as carbonyls, carboxyls, epoxides, and hydroxyls at their edges and surface [15], GO nanoribbons are highly soluble in water and polar organic solvents. The cytotoxic effects of these nanomaterials were investigated previously. This study revealed the concentration-dependent cytotoxicity of these nanomaterials [16].

Streptococcus mutans (S. mutans) includes a variety of Gram-positive strains that evolve in close association with the human host [17]. The easy access to oral samples from human volunteers and the ability to identify the significant contributors to health and disease has led to discovering some bacterial interactions due to the formation of oral biofilms. S. mutans is an oral pathogen that is found on the teeth [18]. This agent of human dental caries has the capacity to produce large quantities of organic acids and outcompete non-cariogenic commensal species at low pH conditions [19–23]. The antibiofilm activity of GO nanoribbons has not been related to the physicochemical properties of these nanomaterials, previously [24–26].

In this paper, the antibiofilm effect of GO nanoribbons related to their surface physicochemical properties is reported. This investigation confirms the potential of these nanomaterials for further use in biomedical applications.

3 Research Methodology

The preparation of Trypticase yeast extract (TYE) medium, solutions of glucose and sucrose (Difco), phosphate-buffered saline (PBS) buffer (pH 7.2) was reported in our previous work [27]. 2 mg/ml GO nanoribbons were purchased from Sigma.

The preparation of the biofilms and their staining were explained in our previous work [27].

After 4 hours of incubating the bacteria in the Fluorescence Correlations Spectroscopy (FCS) cells with the GO nanoribbons, BacLight kit solutions were used to determine the ratio of dead to living cells. The preparation of the kit solutions and imaging of bacterial biofilms after their incubation with GO nanoribbons were previously described. A confocal laser scanning microscope (Leica TCS SP5) was used for imaging [27]. The biofilms that were not incubated with GO nanoribbons were used as control. The experiments of the antibiofilm effect of GO were carried out six times in triplicata.

A transmission electron microscope (TEM) JEOL JEM 2100F was used for the study of the electronic structure of GO nanoribbons [28].

A Thermo Scientific model Perkin Elmer spectrum 65 FTIR spectrometer with an attenuated total absorbance probe was used in the range of 600-4000 cm^{-1} available on the equipment for the analysis of GO nanoribbons and FTIR spectra at 4 cm^{-1} resolution were recorded with 32 scans co-added to improve the signal to noise ratio (S/N) [27, 29].

Positive and negative ion spectra were obtained on an ION-TOF IV time-of-flight secondary ion mass spectrometer (TOF-SIMS) as previously described [27, 30].

The Student's t-test was used to compare one sample mean on a measure with another sample mean on the same measure. The p-value and confidence level were determined. The outcome of the test was used to draw inferences about how different the samples were from each other. The p-values were obtained to check the patterns of the interactions among the variables of experiments. A p-value of less than 0.05 was considered statistically significant for our data [31].

4 Results

4.1 FTIR analysis of GO nanoribbons

The peaks in the FTIR spectra of GO nanoribbons before and after their incubation with bacterial biofilms were determined. Figure 1 shows the FTIR spectrum of GO nanoribbons.

Broadband and a sharp peak were observed at 3350 cm^{-1} and 1650 cm^{-1}. These peaks were attributed to the OH stretching, and bending vibrations of water molecules adsorbed on GO nanoribbons, respectively [32]. The same peaks appeared in the spectrum of the samples after incubation with bacterial biofilms.
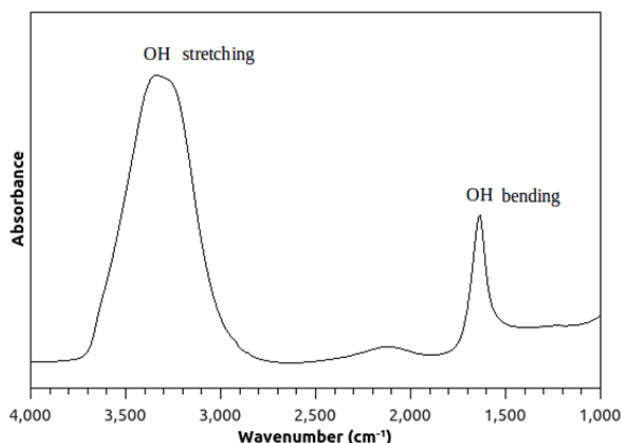
Figure 1 – FTIR spectrum of GO nanoribbons including broadband at 3350 cm^{-1} and a sharp peak at 1650 cm^{-1} corresponding to OH stretching and bending vibrations of water molecules, respectively

The intensity of the broadband at 3350 cm^{-1} decreased in the spectrum of the sample incubated with the biofilms, whereas the intensity of the sharp peak at 1650 cm^{-1} increased due to the incubation of the samples with the bacterial medium (results not shown).

Figure 2 shows the peak intensity ratios of the spectra of GO nanoribbons before and after incubation with the biofilms.
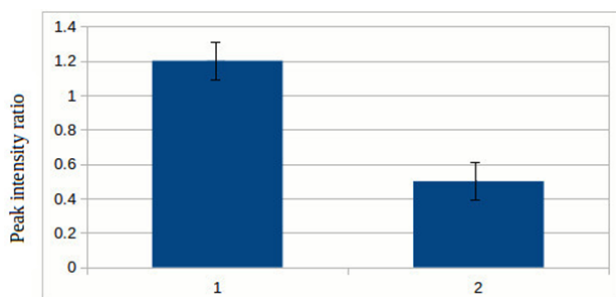

Figure 2 – The peak intensity ratios of the spectrum of GO nanoribbons after incubation with the biofilms to that of the spectrum of the samples before incubation with the bacterial medium

The peak intensity ratios of the OH bending and stretching vibrations of water molecules adsorbed on GO nanoribbons are indicated with 1 and 2, respectively.

4.2 TEM imaging of GO nanoribbons

The TEM imaging of GO nanoribbons showed their planar structure. The nano-sized crystalline layers of GO bent on themselves were observed on carbon support (Figure 3).

The GO nanoribbons were highly electron transparent. In Figure 3a, several folded sheets of these nanomaterials are observed. Figure 3b shows the nanometric size of the sheet border of the sample. The estimated thickness of the sheet could vary between 5 nm and 20 nm.
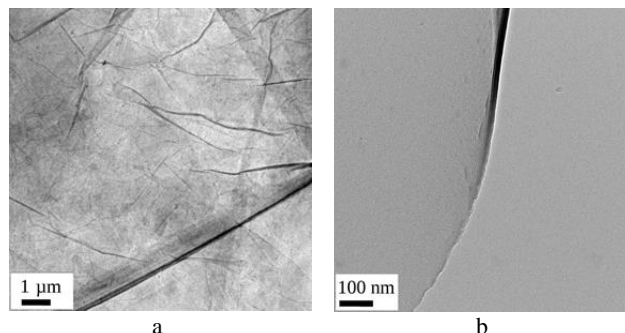

Figure 3 – TEM images of (a) folded sheets and (b) sheet border of GO nanoribbons

The surface properties and bactericidal effects of the GO nanoribbons using TOF-SIMS and confocal microscopy for imaging bacterial biofilms were investigated, respectively.

4.3 Fluorescence imaging of GO nanoribbons

Figure 4 shows the antibiofilm activity of the GO nanoribbons.

The average thickness of the biofilms was about 10 μm. The dispersion of microcolonies was irregular in exopolymers. The dead and alive bacteria were colored in red and green, respectively.
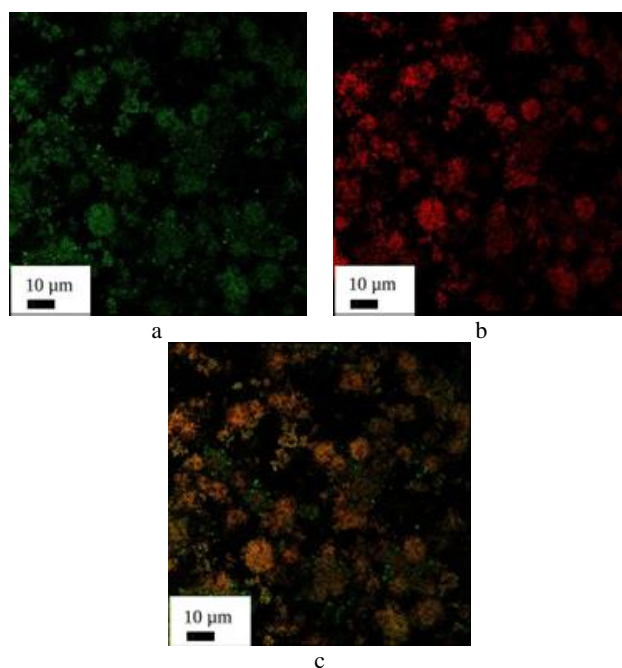

Figure 4 – Antibiofilm activity of GO nanoribbons:
a – green illumination only; b – red illumination only;
c – overlay (both laser excitation wavelengths)

Figure 5 shows the amount of dead and alive bacteria without and with GO nanoribbons in the biofilms.

As seen in Figure 5, a considerable amount of bacteria was killed after 4h of incubation with the GO nanoribbons.
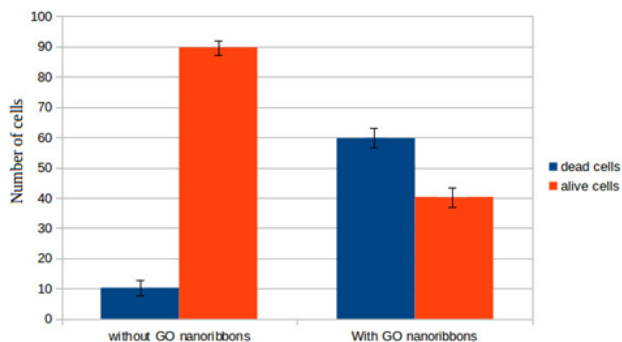
Figure 5 – Amount of dead and alive bacteria in the biofilms without GO nanoribbons (a) and with GO nanoribbons (b)

The antibiofilm activity of the samples with GO nanoribbons was higher than the one without these nanomaterials (controls). The difference in the activity of the samples was 50 % ± 3 %. The high bactericidal activity of these nanomaterials showed a significant effect on biofilms.

4.4 TOF-SIMS analysis

Figure 6 shows the TOF-SIMS spectra of the GO nanoribbons before and after incubation with the biofilms.

Table 1 represents the intensities of the OH^-, O^-, NO_2^- and NO_3^- peaks of GO nanoribbons.

The hydrocarbon peaks and a peak at 23 m/e attributed to Na^+ were observed in the positive mode spectrum (Fig. 6 a).
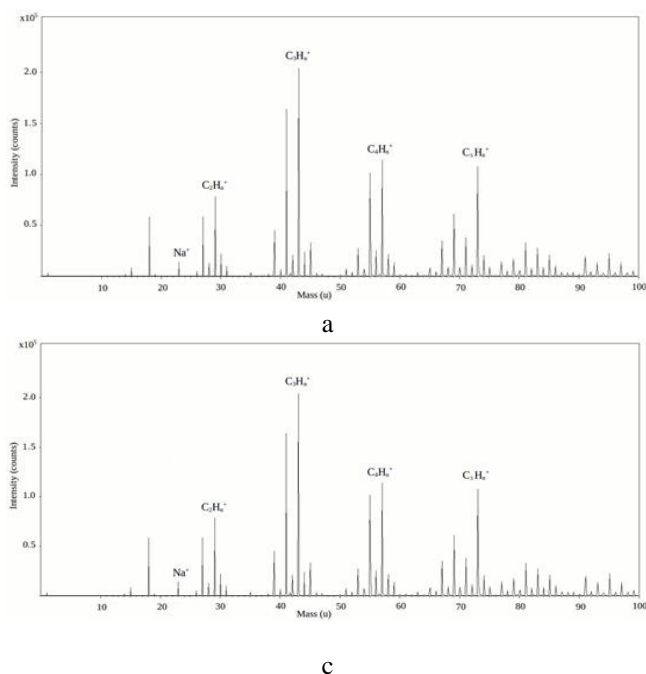
Table 1 – The intensities of the OH^-, O^-, NO_2^- and NO_3^- peaks of GO nanoribbons before (second row) and after their incubation with bacterial biofilms (third row)

OH^-	O^-	NO_2^-	NO_3^-
$1.5 \cdot 10^5$	$2.0 \cdot 10^5$	N/A*	N/A
$1.1 \cdot 10^5$	$1.6 \cdot 10^5$	$2.5 \cdot 10^4$	$1.6 \cdot 10^5$

*N/A (not applicable) corresponds to the sample that was not incubated with biofilm as the NO_2^- and NO_3^- peaks were not present in its negative mode spectrum

The primary peaks O^- (m/e 16), OH^- (m/e 17), C_2^- (m/e 24), C_2H^- (m/e 25) and Cl^- (m/e 35) were also observed in the negative mode spectrum (Fig. 6 b). The peaks O_2^- (m/e 32) and Cl^- (m/e 37) were observed in the logarithmic negative mode spectrum. The peaks at 46 m/e and 62 m/e were attributed to NO_2^- and NO_3^-, respectively (Fig. 6 d).

No significant change was observed in the positive mode of the spectrum of the GO nanoribbons after incubation with the biofilms as the peaks attributed to hydrocarbons adsorbed on the surface of samples masked other peaks (Fig. 6 c). In the negative mode of the spectrum after incubation with the biofilms, the NO_2^- peak and the NO_3^- peak appeared. Moreover, the measured intensities of the OH^- and O^- peaks were attenuated in the presence of the biofilms (20 % attenuation), which was attributed to the interactions of the samples with the biofilms (Fig. 6 d).

Figure 7 shows the OH^-/O^- and NO_3^-/NO_2^- ratios of the peak intensity in TOF-SIMS spectra.
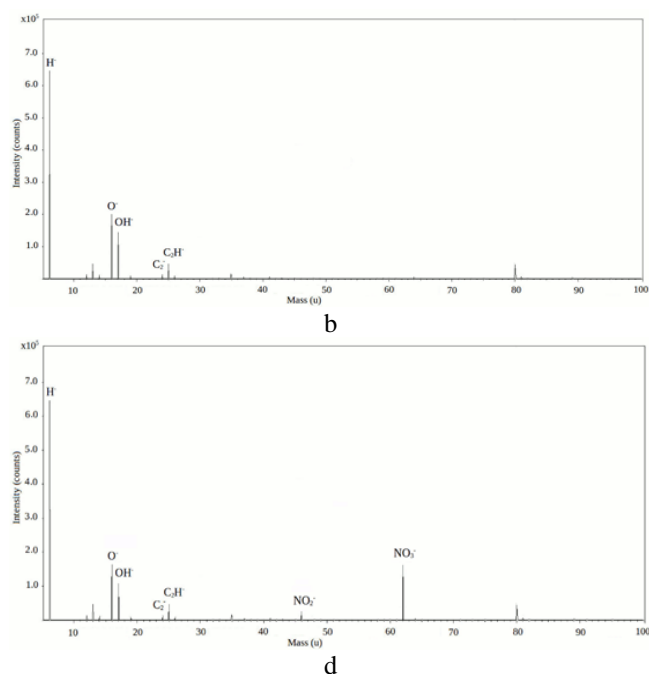

a

b

c

d

Figure 6 – Positive mode and negative mode TOF-SIMS spectra of the GO nanoribbons (a) and (b) before and (c) and (d) after incubation with the biofilms
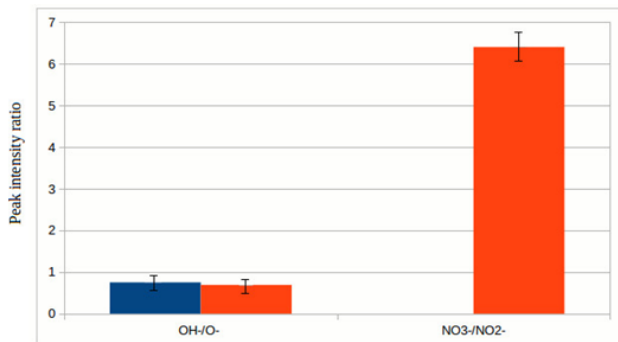
Figure 7 – The OH-/O- and NO3-/NO2- ratios of the peak intensity in TOF-SIMS spectra. The data for samples before and after incubation with biofilms are represented in blue and red, respectively

As shown in Figure 7, the OH^-/O^- ratios of the peak intensities in the negative mode spectra did not have a significant change before and after incubation of samples with biofilms. A considerable value was observed for the NO_3^-/NO_2^- ratio after incubation with biofilms as the peaks were absent in the spectrum before incubation.

5 Discussion

It was expected that GO nanoribbons could have a strong antibiofilm activity as their surface was oxidized according to their TOF-SIMS negative mode spectrum. Therefore, the imaging of biofilms with confocal microscopy was performed to investigate their antibiofilm activity.

GO nanoribbons are being viewed as interesting nanomaterials in microbiology. The synthesis of these nanomaterials from the longitudinal unraveling of MWCNTs using a one-step, one-pot pressurized oxidation reaction or the splitting of MWCNTs by intercalation of potassium metal at elevated temperature help prepare nanomaterials with unique physicochemical properties.

FTIR spectroscopy is one of the most important techniques for the study of the chemical composition of materials. The decrease in the intensity of the band at 3350 cm^{-1} and the increase in the intensity of the peak at 1650 cm^{-1} after the incubation of the GO nanoribbons with the biofilms were attributed to the interaction of these nanomaterials with the biofilms (Fig. 1). The investigation of the peak intensity ratios is an appropriate method to determine if any change has occurred in the samples or on their surface. Our investigation revealed the variations of the OH bending and stretching vibrations of water molecules adsorbed on GO nanoribbons (Fig. 2). The strong hydrophilicity of these nanomaterials makes them appropriate for enhancing water flux in membrane applications [33].

The size and morphology of nanomaterials are key factors that have an important role in their bactericidal effects. The folded sheets of GO nanoribbons and their nanometric size were investigated in this study. The thickness of the sheets was not the same and could vary on different spots (Fig. 3). Several studies revealed that the antibacterial activity was particle size-dependent. Some of the nanomaterials also exhibit a shape-dependent interaction with the bacterial cells [34–36]. It can help explain why the antibiofilm effect of the GO nanoribbons, that do not have a spherical shape, on S. mutans is higher than that of the spherical-shaped nanoparticles.

Our previous study on S. mutans revealed that the average thickness of the biofilms after extensive washing was about 15 µm [27]. The average thickness of the biofilms incubated with the GO nanoribbons was 10 µm (Fig. 4). The incubation with these nanomaterials reduced the size of the biofilms. This is due to the toxicity effect of the GO nanoribbons and the fact that the bacteria in the biofilm structure did not tolerate this incubation (Fig. 5).

Previously, we studied the surface properties of a sample of GO nanoribbons prepared from MWCNTs by TOF-SIMS. Our work showed some sulfur-containing impurities due to the SO^- and SO_2^- ions observed in the negative mode spectra [16]. We did not observe these ions in the negative mode spectra of the GO nanoribbons (Fig. 6). This result shows a cleaner surface of the product purchased from Sigma in comparison to that of the previously studied sample that was synthesized using an oxidative unzipping of MWCNTs. Our investigation on the peak intensity ratios of GO nanoribbons revealed that the OH^-/O^- ratio was the same whereas the NO_3^-/NO_2^- ratio could vary before and after incubation with biofilms. The presence of nitrogen atoms on the surface of these nanomaterials is attributed to the amino acids that are found in the biofilms and can be observed in the vicinity of the sheets of GO nanoribbons (Fig. 7). The change in the peak intensity ratio highlights the chemical modification on a surface of materials [37, 38].

The surface charge of the GO nanoribbons also has an additional effect on their antibiofilm activity. In fact, the oxidative stress on bacterial cells in the biofilms can be due to the surface properties of these nanomaterials. The smooth surface of GO nanoribbons can prevent the adhesion of bacteria to a moderate level, which allows the initial aggregation of bacteria only at the place of seeding the colony and mediating the growth locally, creating a partially covered surface and inhibiting growth [24].

Gram-positive and Gram-negative bacterial strains have different membrane structures. A thin peptidoglycan cell wall surrounds gram-negative bacteria. This wall, in turn, is surrounded by an outer membrane containing lipopolysaccharide. Gram-positive bacteria lack an outer membrane. However, these bacterial strains are surrounded by layers of peptidoglycan many times thicker than is found in the Gram-negatives [39, 40]. When incubated with the biofilms, the GO nanoribbons first penetrate the biofilms and then to the bacterial membrane. It is expected that these nanomaterials have different penetration rates depending on the type of bacterial strains. In other words, their penetration time to the S. mutans membrane is expected to be different from that of the other bacterial strains. The study of the

penetration of GO nanoribbons into the membrane of this bacterial strain is required to understand the antibiofilm activity of these nanomaterials better.

Reactive oxygen species (ROS) are produced when metallic oxide nanoparticles penetrate bacteria. Several studies revealed that the production of ROS induces genetic variability and, with the potential to cause oxidative damage to DNA, proteins, lipids, and other cellular components, promote cell death in specific biofilm regions [41–43]. Further investigation is needed to determine which ROS is produced in S. mutans after incubation with the GO nanoribbons and how much it depends on the incubation time with the biofilm.

Recent investigations have been carried out on the structure, morphology, and physical properties of materials made of W, Ag, Ta, and Ni [44, 45, 46, 47, 48, 49, 50] and the model of their spin-polarized electron transfer [51]. The antibiofilm activities of these materials are required to be investigated.

6 Conclusions

This study reports the antibiofilm effect of GO nanoribbons against the pathogens S. mutans related to their physicochemical properties. FTIR, TEM, and TOF-SIMS characterized these nanomaterials. Their characterization by TEM showed their nanosized planar structure with folded sheets. The FTIR spectroscopy and TOF-SIMS confirmed the presence of water molecules and oxygen-containing ions on GO nanoribbons, respectively. As expected, we observed the folded structure of the samples. Incubation with GO nanoribbons reduced the size of the biofilms.

Moreover, the GO nanoribbons had a high bactericidal effect on biofilms. This could be due to the presence of the oxygen atoms on the surface of these nanomaterials. The incubation of GO nanoribbons with bacterial biofilms affected the physicochemical properties of the samples. The bactericidal effect of these nanomaterials with antimicrobial properties could represent a successful alternative for killing bacteria with the biofilm formation on medical devices. These nanomaterials can also be used with enhanced bactericidal effects on clinically relevant materials such as the tools for oral biopsies and lavage extracts as well as for preparing sterile surfaces for medical applications.

References

1. Goossens, H., Ferech, M., Vander-Stichele, R., Elseviers, M. (2005). Outpatient antibiotic use in Europe and association with resistance: a cross-national database study. *Lancet*, Vol. 365(9459), pp. 579–587, doi: 10.1016/S0140-6736(05)17907-0.

2. Motta, R. N., Oliveia, M., Megalhaes, P. S. F., Dias, A. M., Aragao, L. P., Forti, A. C., Carvalho, C. B. (2003). Plasmid mediated extended spectrum beta lactamase producing strains of enterobacteriaceae isolated from diabetes foot infections in a Brazilian diabetic centre. *Brazilian Journal of Infectious Diseases*, Vol. 7(2), pp. 1024–1032, doi: 10.1590/s1413-86702003000200006.

3. Todar, K. (2008). Bacterial resistance to antibiotics In *Principles of bacterial pathogenesis*, Todar's Online Textbook of Bacteriology Vol. 304, pp. 1421–1423.

4. Flemming, H. C., Wingender, J. (2010). The Biofilm Matrix. *Nature Reviews Microbiology*, Vol. 8(9), pp. 623–633, doi: 10.1038/nrmicro2415.

5. Flemming, H. C., Neu, T. R., Wozniak, D. J. (2007). The EPS matrix: The "house of biofilm cells". *Journal of Bacteriology*, Vol. 189(22), pp. 7945–7947, doi: 10.1128/JB.00858-07.

6. Sutherland, I. W. (2001). Biofilm exopolysaccharides: a strong and sticky framework. *Microbiology*, Vol. 147(Pt 1), pp. 3–9, doi: 10.1099/00221287-147-1-3.

7. Ryder, C., Byrd, M., Wozniak, D. J. (2007). Role of polysaccharides in *pseudomonas aeruginosa* biofilm development. *Current Opinion in Microbiology*, Vol. 10(6), pp. 644–648, doi: 10.1016/j.mib.2007.09.010.

8. Götz, F. (2002). Staphylococcus and biofilms. *Molecular Microbiology*, Vol. 43(6), pp. 1367–1378, doi: 10.1046/j.1365-2958.2002.02827.

9. Vaningelgem, F., Zamfir, M., Mozzi, F., Adriany, T., Vancanneyt, M., Swings, J., De Vuyst, L. (2004). Biodiversity of exopolysaccharides produced by *Streptococcus thermophilus* strains is reflected in their production and their molecular and functional characteristics. *Applied and Environmental Microbiology*, Vol. 70(2), pp. 900–912, doi: 10.1128/aem.70.2.900-912.2004.

10. Lemos, J. A., Quivey, Jr. R. G., Koo, H., Arbanches, J. (2013). Streptococcus mutans*: a new Gram-positive paradigm. *Microbiology*, Vol. 159(3), pp. 436–445, doi: 10.1099/mic.0.066134-0.

11. Higginbotham, A. L., Kosynkin, D. V., Sinitskii, A., Sun, Z., Tour, J. M. (2010). Lower-defect graphene oxide nanoribbons from multiwalled carbon nanotubes. *ACS Nano*, Vol. 4(4): pp. 2059–2069, doi: 10.1021/nn100118m.

12. Han, M. Y., Oezyilmaz, B., Zhang, Y., Kim, P. (2007). Energy band-gap engineering of graphene nanoribbons. *Physical Review Letters*, Vol. 98(20), pp. 206805–206812, doi: 10.1103/PhysRevLett.98.206805.

13. Li, X., Wang, X., Zhang, L., Lee, S., Dai, H. (2008). Chemically derived, ultrasmooth graphene nanoribbon semiconductors. *Science*, Vol. 319(5867), pp. 1229–1232, doi: 10.1126/science.1150878.

14. Jiao, L., Zhang, L., Wang, X., Diankov, G., Dai, H. (2009). Narrow graphene nanoribbons from carbon nanotubes. Nature, Vol. 458(7240), pp. 877–880, doi: 10.1038/nature07919.

15. Lerf, A., He, H., Forster, M., Klinowski, J. (1998). Structure of graphite oxide revisited. *Journal of Physical Chemistry B*, Vol. 102, pp. 4477–4482, doi: 10.1021/jp9731821.

16. Mbeh, D. A., Akhavan, O., Javanbakht, T., Mahmoudi, M., Yahia, L. H. (2014). Cytotoxicity of protein corona-graphene oxide nanoribbons on human epithelial cells. *Applied Surface Science*, Vol. 320, pp. 596–601, doi: 10.1021/nn200021j.

17. Loesche, W. J. (1986). Role of *Streptococcus mutans* in human dental decay. *Microbiological Reviews*, Vol. 50(4), pp. 353–380, doi: 0146-0749/86/040353.

18. Cao, L., Zhang, Z. -Z., S. -B., Xu, Ma, M., Wei, X. (2017). Farnesol inhibits development of caries by augmenting oxygen sensitivity and suppressing virulence-associated gene expression in *Streptococcus mutans*. *The Journal of Biomedical Research*, Vol. 31(4), pp. 333–343, doi: 10.7555/JBR.31.20150151.

19. Banas, J. A., Vickerman, M.M. (2003). Glucan-binding proteins of the oral *streptococci*. *Critical Reviews in Oralal Biology and Medicine*, Vol. 14(2), pp. 89–99, doi: 10.1177/154411130301400203.

20. Bowen, W. H., Koo, H. (2011). Biology of *Streptococcus mutans*-derived glucosyltransferases: role in extracellular matrix formation of cariogenic biofilms. *Caries Research*, Vol. 45(1): pp. 69–86, doi: 10.1159/000324598.

21. Gross, E. L., Beall, C. J., Kutsch, S. R., Firestone, N. D., Leys, E. J., Griffen, A. L. (2012). Beyond *Streptococcus mutans*: dental caries onset linked to multiple species by 16S rRNA community analysis. *PLOS One*, Vol. 7(10), e47722, doi: 10.1371/journal.pone.0047722.

22. Lemos, J. A., Abranches, J., Burne, R. A. (2005). Responses of cariogenic streptococci to environmental stresses. *Current Issues in Molecular Biology*, Vol. 7(1), pp. 95–107, doi: 10.21775/cimb.007.095.

23. Quivey, R. G., Kuhnert, W. L., Hahn, K. (2001). Genetics of acid adaptation in oral *streptococci*. *Critical Reviews in Oral Biology and Medicine*, Vol. 12(4), pp. 301–314, doi: 10.1177/10454411010120040201.

24. Yadav, N., Dubey, A., Shukla, S., Saini, C. P., Gupta, G., Priyadarshini, R., Lochab, B. (2017). Graphene oxide coated surface: Inhibition of bacterial biofilm formation due to specific surface-interface interactions. *ACS Omega*, Vol. 2(7), pp. 3070–3082, doi: 10.1021/acsomega.7b00371.

25. Mokkapati, V. R. S. S., Pandit, S., Kim, J., Martensson, A., Lovmar, M., Westerlund, F., Mijakovic, I. (2018). Bacterial response to graphene oxide and reduced graphene oxide integrated in agar plates. *Royal Society Open Science*, Vol. 5(11), pp. 181083–1810092, doi: 10.1098/rsos.181083.

26. Fallatah, H., Elhaneid, M., Ali-Boucetta, H., Overton, T. W., El Kadri, H. (2019). Antibacterial effect of graphene oxide (GO) nano-particles against *Pseudomonas putida* biofilm of variable age. *Environmental Science and Pollution Research*, Vol. 26(24), pp. 25057–25070, doi: 10.1007/s11356-019-05688-9.

27. Javanbakht, T., Laurent, S., Stanicki, D., Wilkinson, K. J. (2016). Relating the surface properties of superparamagnetic iron oxide nanoparticles (SPIONs) to their bactericidal effect towards a biofilm of *Streptococcus mutans*. *PLOS One*, Vol. 11(4), e0154445, doi: 10.1371/journal.pone.0154445.

28. Choi, E. Y., Han, T. H., Hong, J., Kim, J. E., Lee, S. H., Kim, H. W., Kim, S. O. (2010). Noncovalent functionalization of graphene with end-functional polymers. *Journal of Materials Chemistry*, Vol. 20(10), pp. 1907–1912, doi: 10.1039/b919074k.

29. Javanbakht, T., Bérard, A., Tavares, J. R. (2016). Polyethylene glycol and poly(vinyl alcohol) hydrogels treated with photo-initiated chemical vapor deposition. Canadian Journal of Chemistry, Vol. 94(9), pp. 744–750, doi: 10.1139/cjc-2016-0229.

30. Javanbakht, T., Laurent, S., Stanicki, D., David, E. (2019). Related physicochemical, rheological, and dielectric properties of nanocomposites of superparamagnetic iron oxide nanoparticles with polyethyleneglycol. *Journal of Applied Polymer Science*, Vol. 137(3), pp. 48280–48289, doi: 10.1002/app.48280.

31. El-Naggar, N. E., Abdelwahed, N. A. M. (2014). Application of statistical experimental design for optimization of silver nanoparticles biosynthesis by a nanofactory *Streptomyces viridochromogenes*. *Journal of Microbiology*, Vol. 52(1), pp. 53–63, doi: 10.1007/s12275-014-3410-z.

32. Suneetha, R. B. (2018) Spectral, thermal and morphological characterization of biodegradable graphene oxide chitosan nanocomposites. *Journal of Nanoscience and Technology*, Vol. 4(2), pp. 342–344, doi: 10.30799/jnst.sp208.18040201.

33. Ammar, A., Al-Enizi, A. M., AlMaadeed, M. A., Karim, A. (2016). Influence of graphene oxide on mechanical, morphological, barrier, and electrical properties of polymer membranes. *Arabian Journal of Chemistry*, Vol. 9(2), pp. 274–286, doi: 10.1016/j.arabjc.2015.07.006.

34. Morones, J. R., Elechiguerra, J. L., Camacho, A., Holt, K., Kouri, J. B., Ramırez, J. T., Yacaman, M.J. (2005). The bactericidal effect of silver nanoparticles. *Nanotechnology*, Vol. 16(10), pp. 2346–2353, doi: 10.1088/0957-4484/16/10/059.

35. Rai, R. V., Bai, J. A. (2011). Nanoparticles and their potential application as antimicrobials. Science against microbial pathogens: Communicating Current Research and Technological Advances, In Méndez-Vilas, A. (Ed.), Formatex Research Center, Spain, *Microbiology Series*, Vol. 1(3), pp. 197–209.

36. Pal, S., Tak, Y .K., Song, J. M. (2007). Does the antimicrobial activity of silver nanoparticles depend on the shape of the nanoparticle? A study of the Gram-negative bacterium *Escherichia coli*. *Applied Environmental Microbiology*, Vol. 73(6), pp. 1712–1720, doi: 10.1128/AEM.02218-06.

37. Goacher, R. E., Tsai, A. Y. -L., Master, E. R. (2013). Towards practical time-of-flight secondary ion mass spectrometry lignocellulolytic enzyme assays. *Biotechnology for Biofuels*, Vol. 6(1), pp. 132–144, doi: 10.1186/1754-6834-6-132.

38. Mou, H. L., Wu, S., Fardim, P. (2016). Applications of ToF-SIMS in surface chemistry analysis of lignocellulosic biomass: A review. *BioResearch*. Vol. 11(2), pp. 5581–5599, doi: 10.15376/biores.11.2.

39. Silhavy, T. J., Kahne, D., Walker, S. (2010). The bacterial cell envelope. *Cold Spring Harbor Perspectives in Biology*. Vol. 2(5), a000414, doi: 10.1101/cshperspect.a000414.

40. Beveridge, T. J. (1999). Structures of Gram-negative cell walls and their derived membrane vesicles. *Journal of Bacteriology*, Vol. 181(16), pp. 4725–4733, doi: 0021-9193/99.

41. Dwivedi, S., Wahab, R., Khan, F., Mishra, Y. K., Musarrat, J., Al-Khedhairy, A. A. (2014). Reactive oxygen species mediated bacterial biofilm inhibition via zinc oxide nanoparticles and their statistical determination. *PLOS One*, Vol. 9(11), e111289, doi: 10.1371/journal.pone.0111289.

42. Cap, M., Vachova, L., Palkova, Z. (2012). Reactive oxygen species in the signaling and adaptation of multicellular microbial communities, *Oxidative Medicine and Cellular Longevity*, Vol. 2012(11), pp. 976753–976765, doi: 10.1155/2012/976753.

43. Santos, C. L., Albuquerque, A. J. R., Sampaio, F. C., Keyson, D. (2013). Nanomaterials with antimicrobial properties: applications in health sciences. Microbiological pathogens and strategies for combatting them. *Science, Technology and Education*, In Méndez-Vilas, A. (Ed.), Vol. 1(4), pp. 143–154.

44. Hoseinzadeh, S., Ghasemiasl, R., Bahari A. Ramezani, A. H. (2018) Effect of post-annealing on the electrochromic properties of layer-by-layer arrangement FTO-WO_3-Ag-WO_3-Ag. *Journal of Electronic Materials*, Vol. 47, pp. 3552–3559, doi: 10.1007/s11664-018-6199-4.

45. Ramezani, A. H., Hoseinzadeh, S., Bahari A. (2018) The effects of nitrogen on structure, morphology and electrical resistance of tantalum by ion implantation method. *Journal of Inorganic and Organometallic Polymers and Materials*, Vol. 28, pp. 847–853, doi: 10.1007/s10904-017-0769-4.

46. Hoseinzadeh, S., Ghasemiasl, R., Bahari A. Ramezani, A. H. (2017) n-type WO_3 semiconductor as a cathode electrochromic material for ECD devices. *Journal of Materials Science: Materials in Electronics*, Vol. 28, pp. 14446–14452, doi:10.1007/s10854-017-7306-7.

47. Hoseinzadeh, S., Ghasemiasl, R., Bahari A. Ramezani, A. H. (2017) The injection of Ag nanoparticles on surface of WO_3 thin film: enhanced electrochromic colorationn efficiency and switching response. *Journal of Materials Science: Materials in Electronics*, Vol. 28, 14855–14863, doi: 10.1007/s10854-017-7357-9.

48. Hoseinzadeh, S., Ramezani, A. H. (2019) Tantalum/nitrogen and n-type WO_3 semiconductor/FTO structures as a cathode for the future of nanodevices. *Journal of Nanostructure*, Vol. 9, pp. 276–286, doi:10.22052/JNS.2019.02.010.

49. Hoseinzadeh, S., Ramezani, A. H. (2019) Investigation of Ta/NII-WO_3/FTO structures as a semiconductor for the future of nanodevices. *Journal of Nanoelectronics and Optoelectronics*, Vol. 14, pp. 1413–1419, doi: 10.1166/jno.2019.2564.

50. Hoseinzadeh, S., Ramezani, A. H. (2018) Corrosion performance of Ta/Ni ions implanted with WO_3/FTO, *Journal of the Chinese Society of Mechanical Engineers*, Vol. 39(5), pp 501–507.

51. Ramezani, A. H., Hoseinzadeh, S., Ebrahiminejad, Z. H., Masoudi, S. F., Hashemizadeh A. (2020) Spin-polarized electron transfer in multilayers with different types of rough interfaces. *Journal of Superconductivity and Novel Magnetism*, doi: 10.1007/s10948-019-05335-x.